

Simple correction to bandgap problems in IV and III-V semiconductors: an improved, local first-principles density functional theory

Sujoy Datta,^{1,2} Prashant Singh,^{3,*} Chhanda B. Chaudhuri,² Debnarayan Jana,¹ Manoj K. Harbola,⁴ Duane D. Johnson,^{3,5} and Abhijit Mookerjee^{2,6}

¹Department of Physics, University of Calcutta, Kolkata 700009, India

²Department of Physics, Lady Brabourne College, Kolkata 700017, India

³Ames Laboratory, U.S. Department of Energy, Iowa State University, Ames, Iowa 50011 USA

⁴Department of Physics, Indian Institute of Technology, Kanpur, 208016, India

⁵Department of Materials Science & Engineering, Iowa State University, Ames, Iowa 50011, USA

⁶S. N. Bose National Centre for Basic Sciences, Salt Lake City, Kolkata 700098, India

(Dated: December 14, 2024)

We report results from a fast, efficient and first-principles full-potential N^{th} -order muffin-tin orbital (FP-NMTO) method combined with van Leeuwen-Baerends correction to local density approximation exchange-correlation potential. We show that more complete and compact basis set is critical in improving the electronic and structural properties. We exemplify the self-consistent (non-relativistic) FP-NMTO calculations on group IV and III-V semiconductors. Notably, predicted bandgap, lattice constant, and bulk modulus are in good agreement with experiments (e.g., for Ge we find 0.86 eV, 5.57Å, 75 GPa vs. measured: 0.74 eV, 5.66Å, 77.2 GPa). We also showcase its application to the electronic properties of 2-dimensional h -BN and h -SiC, again finding good agreement with experiments.

I. INTRODUCTION

Semiconducting materials have always been of great interest due to their central role in modern electronics.¹⁻⁷ In this era of designing optimal materials, it has become essential to estimate quickly and accurately the bandgaps of such materials. Experimentally we also would benefit from an efficient computational tool for predicting bandgaps (among many other properties) prior to synthesis. We consider the problem of predicting bandgaps to be solved by a computational method that delivers an accurate result for compounds spanning the whole periodic table and is simultaneously practical to compute. Standard exchange correlation (XC) functionals to density functional theory (DFT), such as local density approximation (LDA) and generalized gradient approximation (GGA)^{8,9} have been the backbone of DFT-based calculations for decades. Unfortunately, the unphysical self-Coulomb repulsion¹⁰ leads to a systematic underestimation of bandgaps.¹¹⁻¹³

In semiconductors, the fundamental bandgap is the difference of ionization energy ($I = E(N) - E(N - 1)$) and electron affinity ($A = E(N + 1) - E(N)$). This involves the knowledge of the total energies of states with $(N - 1)$, N , $(N + 1)$ electrons, where $E(N + 1)$ involves explicit knowledge of excited state. However, in the traditional Kohn-Sham (KS) density functional theory (DFT),¹⁴ the I and A are approximated as the negative of the top of the valence band (HOMO) and the negative of conduction band minimum (LUMO) of the same N electron system. The presence of derivative discontinuity (Δ_{xc}) in the definition of fundamental bandgap, $E_{gap} = E_{gap}^{KS} + \Delta_{xc}$, breaks that assumption.^{15,16} If I and A could be found exactly for an infinite system, the KS gap ($E_{gap}^{KS} = E_I - E_A$) would be same as Fundamental

gap ($E_{gap} = I - A$).

The difference between the E_{gap}^{KS} and the E_{gap} is the discontinuous change in the Kohn-Sham potential by a constant Δ_{xc} .¹⁷ The designation of Δ_{xc} in DFT is often refer to the discontinuous jumps in the derivative of the total energy with respect to particle number,¹⁹ as the time average of the total number of electrons in any interacting system can be a fraction.¹⁸ Although the LDA exchange energy has a derivative discontinuity at certain integer electron numbers, but the potential shows no such discontinuity.²⁰ For the LDA or semi-local functionals, e.g. GGA^{8,9}, the discontinuity could be as large as 50% or even more and no straightforward method exists to estimate Δ_{xc} .²¹

In the recent past, many accurate semi-local XC functionals have been constructed by introducing increasingly complex density dependence,^{22,23} which satisfy a number of exact physical behaviors. If any approximate (e.g. semi-local) functional can reproduce the exact asymptotic behavior of the potential then it is good enough for extracting the information of excited state.²⁴⁻²⁶ Based on these arguments, some semi-empirical functionals are derived and implemented within DFT formalism as correction to the local density approximation (LDA) exchange.^{20,21,26-34} These functionals which incorporate density gradients such that the potential is asymptotically well behaved,^{21,33-36} are mathematically easy to handle and often produced good results without much computational cost.^{27,34,36} Similarly, accurate exact-exchange functionals with variations that approach the form enforced by LDA+vLB have appeared,³⁷ but not yet explored for solids.

Here we use the vLB corrected LDA in self-consistent full-potential N^{th} -order muffin-tin orbital (FP-NMTO) method. The FP-NMTO uses compact basis set to describe the entire system including the interstitial, and it

is accurate whether or not the system is close-packed. The error coming in the process of making energy independent basis set is also minimized in FP-NMTO, which is in contrast to Tight-Binding Linearized muffin-tin orbital (TB-LMTO-ASA).^{38–42} The FP-NMTO utilizes the interpolation of higher-order energy derivatives of Taylor’s expansion of basis set^{43–46} and provide a smaller and energy-independent self-consistent basis set. The FP-NMTO basis set is comparable to localized Wannier functions – a prerequisite for computational speed and efficiency. We exemplify our approach through electronic structure and bandgap calculation of group IV and III-V semiconductors.

II. COMPUTATIONAL METHOD

We apply self-consistent FP-NMTO-vLB approach to calculate electronic properties of group IV and III-V semiconductors, and discuss Ge and GaAs. We compare FP-NMTO calculated bandgaps using LDA,⁴⁷ PBE,⁸ and LDA+vLB²⁴ with experiments and other existing theories. In FP-NMTO, we use third-order correction to the energy derivatives of wave functions ($N = 3$) to make the energy independent basis set. We use $8 \times 8 \times 8$ k-point mesh (29 irreducible points) for Brillouin zone sampling. The self-consistent potential converged to a difference of 10^{-6} after several tens of iterations. In calculating the lattice constant, we utilized a least square fit of our data to the Murnaghan’s equation of state.⁴⁸ The FP-NMTO+vLB calculated equilibrium lattice constants are in good agreement with the experiments.^{49,50} All calculations are done self-consistently and non-relativistically. To facilitate convergence, we have used Andersen mixing. The k-space integration is done using the tetrahedron method (for more description of TB-LMTO-ASA see appendix).

III. THEORETICAL DETAIL

The MT-potential and partial-wave solutions: LMTO vs NMTO

In the TB-LMTO-ASA, atomic spheres are used to describe both the variation of electronic charge and the potential. These spheres need to be space filling with minimal (optimal) overlap ($\leq 15\%$). Overlap is essential for atomic bonding, whereas too large an overlap of charge may lead to its over-counting. The potential for a given atom is reasonably long ranged but the atomic charge density is more localized around the ion cores. However, NMTO has two different classes of concentric spheres: potential (MT/ASA) spheres of radius s and charge spheres (screening/hard spheres) of radius a , whereas $a < s$, see Fig.1(b). However, the overlap of potential spheres in NMTO can be as large as 50% so

full potential approach is a pre-requisite both in atomic spheres and interstitials.

The solutions of radial KS equations [Eq. 4] for atomic-potential φ^{as} is continued from the core of atom towards the muffin-tin surfaces at $r = s$. This is matched with the solution for a flat part of potential (as in LMTO, this flat potential is taken as zero potential) φ^{int} , which is denoted by φ^0 . The φ^0 is valid up to the boundary of hard sphere surface ($r = a$). We normalize at the boundary of hard sphere surface (a) such that $\varphi^0|_a = 1$. The normalized wave-functions have superscript “a”:

$$\begin{aligned}\varphi_{R,l}^a(\epsilon, r) &\equiv \frac{\varphi_{R,l}(\epsilon, r)}{\varphi_{R,l}^0(\epsilon, a_R)} \\ \varphi_{R,l}^{0a}(\epsilon, r) &\equiv \frac{\varphi_{R,l}^0(\epsilon, r)}{\varphi_{R,l}^0(\epsilon, a_R)}\end{aligned}\quad (1)$$

The $\varphi_{R,l}^{0a}(\epsilon, r)$ is matched with screened spherical waves (SSW: ψ^a) continuously but with a kink at a and truncated in the region $a_R \leq r \leq s_R$. $\varphi_{R,l}(\epsilon, r)$ is truncated outside $0 \leq r \leq s_R$. The SSWs grow outwards, which are sorted in two groups depending on the values of (R,l,m): active channels (subscript $A \equiv RL$) and passive channels (subscript $I \equiv RL$). The matching described above is for the active channels which are truncated inside hard spheres with kinks. The passive channels are substituted smoothly by φ^{as} inside hard spheres. Finally, a basis set with elements termed as Kinked Partial Waves (KPW), which are defined in all space, is formed as:

$$\begin{aligned}\phi_{Rlm}^a(\epsilon, r_R) &= [\varphi_{R,l}^a(\epsilon, r_R)_R - \varphi_{R,l}^{0a}(\epsilon, r_R)]Y_{l,m}(\hat{r}_R) \\ &\quad + \psi_{Rlm}^a(\epsilon, r_R)\end{aligned}\quad (2)$$

A linear combination $\sum_{RL \in A} \phi_{Rlm}^a(\epsilon_i, r_R) c_{Rlm,i}^a$ of KPWs is a solution of KS equation but not the individual KPWs. A kink cancellation condition can be achieved such that the kink in any hard sphere is cancelled by the sum of the kinks from the tails of KPWs from neighboring sites.

This basis set spanned by the KPWs is explicitly energy dependent. Energy dependent basis set slows down the calculation which was the problem in exact MTO (EMTO) formalism. In LMTO, energy dependence is removed by a self-consistent choice of energy ϵ_ν about which a Taylor series expansion of basis functions are performed. The series is truncated after first-order term leading to an error $\propto (\epsilon - \epsilon_\nu)^2$ in the solution of KS equation. The energy independent set of basis functions, the so called NMTO are the superposition of KPWs at a mesh of energies (calculated self-consistently) using Newton’s interpolation method such that:

$$\begin{aligned}|\chi^{0\dots N}\rangle &= \sum_{n=0}^N |\phi(\epsilon_n)\rangle L_n^{0\dots N} \\ &= |\phi[0]\rangle + |\phi[01]\rangle (E^{(0\dots N)} - \epsilon_0) + \dots + \\ &\quad |\phi[0\dots N]\rangle (E^{(N-1,N)} - \epsilon_{N-1})(E^{(0\dots N)} - \epsilon_0)\end{aligned}$$

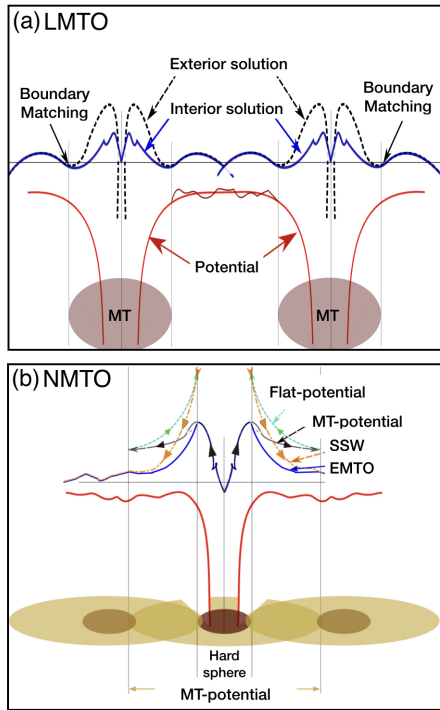


FIG. 1. (Color online) Schematic of atomic spheres and corresponding potential in (a) TB-LMTO-ASA, and (b) FP-NMTO approaches.

where $\phi[0] \equiv \phi(\epsilon_0)$; $\phi[01] \equiv \frac{\phi(\epsilon_0) - \phi(\epsilon_1)}{\epsilon_0 - \epsilon_1}$ are the terms in divided difference table. The error in the solution of KS equation becomes

$$\psi(\mathbf{r}) - \psi(\epsilon, \mathbf{r}) \propto (\epsilon - \epsilon_0)(\epsilon - \epsilon_1) \dots (\epsilon - \epsilon_n) \quad (3)$$

The van Leeuwen Baerends correction to LDA exchange

The Kohn-Sham (KS) equation transforms the interacting many-electron system to a system of non-interacting electrons moving in an effective potential due to all other electrons and ions. Using the Hohenberg-Kohn theorem, the Schrödinger's equation for many body system reduces to the so-called Kohn-Sham equation

$$\mathbf{T}[\rho(\mathbf{r})] + \mathbf{V}[\mathbf{r}] \Psi(\mathbf{r}) = \mathcal{E} \Psi(\mathbf{r}). \quad (4)$$

The total energy-functional having the contribution of this effective potentials is given by

$$\begin{aligned} \mathbf{E} = & - \sum_{\lambda \in occ} \frac{1}{2} \int d\mathbf{r} \Psi_{\lambda}^*(\mathbf{r}) \nabla^2 \Psi_{\lambda}(\mathbf{r}) + \int d\mathbf{r} \rho(\mathbf{r}) V_{ie}(\mathbf{r}) \\ & + \frac{1}{2} \iint d\mathbf{r} d\mathbf{r}' \frac{\rho(\mathbf{r}) \rho(\mathbf{r}')}{|\mathbf{r} - \mathbf{r}'|} + E_{xc}[\rho(\mathbf{r})] \end{aligned} \quad (5)$$

where 1st term is kinetic energy. The 2nd, 3rd, and 4th terms involve the external ion-electron [*ie*], the

Hartree, and exchange-correlation [XC] contributions, respectively, which combine to provide the self-consistently determined effective potential, $V_{eff}(\mathbf{r})$, written as

$$V_{eff}(\mathbf{r}) = V_H[\rho(\mathbf{r})] + V_{ie}[\rho(\mathbf{r})] + V_{xc}[\rho(\mathbf{r})]. \quad (6)$$

Generally, $V_{xc}[\rho(\mathbf{r})]$ is given by the variation of the $E_{xc}[\rho(\mathbf{r})]$ with respect to density $\rho(\mathbf{r})$. The LDA, first introduced by Slater, is based on homogeneous electron gas.⁵¹ It simplifies the non-local exchange energy in terms of the local $\rho^{1/3}$ potential,⁵² as $E_{xc}^{LDA} \simeq \int \rho(\mathbf{r}) \epsilon_{xc}[\rho(\mathbf{r})] d\mathbf{r}$. In semi-local form, it is simplified as $E_{xc}^{semi} \simeq \int \rho(\mathbf{r}) \epsilon_{xc}[\rho(\mathbf{r}); \nabla^{(n)} \rho(\mathbf{r})] d\mathbf{r}$ in terms of local XC energy density. While calculations using DFT potentials from LDA/GGA are the most successful and widespread in the last three decades, most of these calculations have resulted in significant underestimation of the bandgaps of semiconductors and insulators.

Many of the well-established DFT and LDA fail to reproduce the measured energy gaps of semiconducting material due to wrong asymptotic behavior at $r \rightarrow 0$ and $r \rightarrow \infty$ limits.³⁴ The LDA potential decays exponentially similar to density for finite systems, however, the potential should decay as $-1/r$, i.e., Coulomb like.⁵³ Becke proposed a nonlocal correction to the energy-functional and then took the functional derivative to find the exchange potential.²⁶ This gave the correct form of exchange-energy density in the asymptotic region but failed to reproduce the exact behavior for the potential. Perdew and Wang developed generalized gradient approximation (GGA) to the density.^{9,54} Later van Leeuwen and Baerends provides a similar type of correction to the LDA exchange, which improved significantly the eigenvalues for the highest-occupied orbitals of atoms.^{24,55-57} The vLB-corrected LDA potential can be written as

$$v_{xc}(\mathbf{r}) = [v_x^{LDA}(\mathbf{r}) + v_x^{vLB}(\mathbf{r})] + v_c^{LDA}(\mathbf{r}), \quad (7)$$

with

$$v_x^{vLB}(\mathbf{r}) = -\beta \rho^{1/3}(\mathbf{r}) \frac{x^2}{1 + 3\beta x \sinh^{-1}(x)} \quad (8)$$

where $x = \frac{|\nabla \rho(\mathbf{r})|}{\rho^{4/3}(\mathbf{r})}$ and $\beta = 0.05$. This method of gradient correction to the XC-functional is more built into the theory and thus less artificial than self-interaction-corrected (SIC) approaches.^{34,36}

Singh et al.^{34,36} recently discussed the implementation of this method in LMTO-ASA, in particular the vLB matching condition in the interstitial (an asymptotic value within a solid). Additionally, they discussed the comparison to plane-wave implementations, and why the dielectric (or work) function is not required in site-centered methods,³⁴ and how the vLB-correction potential is then able to approach results of hybrid functionals.

The search for a fast semilocal multiplicative XC-potential, which is more universally accurate than those presented before is certainly not an easy task. However, in this respect, it may be helpful to try to understand what is going on in terms of the shape of the potentials

considered in this work. The vLB correction is motivated by the Becke,⁵⁸ which also leads to correct $-1/r$ behavior in the outer regions of finite systems. The potential has been employed in the past to study the effect of the correct asymptotic behavior of the potential on response properties of atoms.²⁴ This shows that an improved exchange-correlation potential which is particularly accurate in the outer regions of the AS gives significantly improved results over the LDA.

The correctness of the eigenvalue of the highest occupied state, the appropriate asymptotic behavior and integer discontinuity of the exchange-correlation potential are all inter-related, which helps to estimate the accurate bandgaps in DFT methods. This is well known that Harbola-Sahani exchange-only functional give accurate upper most eigenvalues and have the correct asymptotic behavior for the finite systems too.^{21,34,60} Similar to the inbuilt derivative discontinuity of exact-exchange⁵⁹ and Harbola-Sahani exchange-only potential,²¹ the vLB also shows similar discontinuities at the “shell-steps” in potential in Fig. 2. Thus, it is not a coincidental that for a large number of systems the exact-exchange, self-Interaction correction and Harbola-Sahani exchange-only potential give significantly improved bandgaps compared to semi-local functionals.^{21,59} We plot, in Fig. 2, the potential for Ge and Si in the atomic sphere. The result provides some guidance when choosing (within the KS method) an exchange-correlation potential that is adequate for the problem at hand, e.g., bandgap calculation in our case. Trends in the results could be understood by comparing the shape of the potentials.

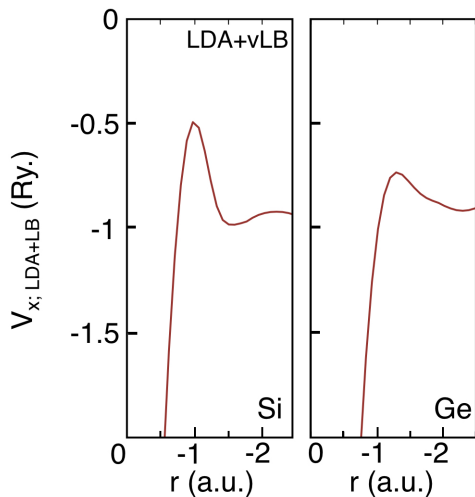


FIG. 2. (Color online) The LDA+vLB exchange potential calculated with FP-NMTO for Si and Ge, which shows good agreement with exact-exchange potential.⁵⁹

The discontinuous shift in the exchange potential turns out to be closely related to the “step structure” of the exchange potential of atoms, also shown by van Leeuwen-Baerends in the proposed model potential.²⁴ Such a step is present regardless of how small the occupancy of a

shell is, as long as it is greater than zero. Hence, in the fractionally filled orbital case, the orbitals are filled with a successively increasing fractional particle number and a new step is created at the exact point when a new shell is opened. If a boundary condition $v_X \rightarrow 0$ as $r \rightarrow \infty$ is enforced for the potential, it shifts the whole potential discontinuously. Krieger, Li, and Iafate⁶¹ observed that with just a tiny fraction of occupancy in a new shell, the exchange potential is shifted discontinuously, where a true exact exchange potential (e.g., van Leeuwen-Baerends) have shows required potential discontinuity.^{61–63} Similar considerations also apply for the time-dependent extension of DFT.^{64,65}

IV. RESULTS AND DISCUSSION

We demonstrate that improving the LDA for its behavior in the outer regions of the atomic sphere and basis set indeed leads to significant improvement in bandgap. We exemplify this by calculating the bandgaps of Si, Ge, GaP, GaSb, GaAs, InAs, InSb and InP and compared them with the existing theory and experiments. For better understanding, we discuss Ge and GaAs results in more detail.

Bulk Germanium: In Fig. 3, we plot the band structure and total density of states (DOS) for Ge. Ge crystallizes in the diamond ($Fd\bar{3}m$) structure.⁶⁶ Two equivalent Ge’s are placed at $(0, 0, 0)$ and $(1/4, 1/4, 1/4)$ in a cubic cell with empty spheres (ES) at $(-1/4, -1/4, -1/4)$ and $(1/2, 1/2, 1/2)$. Both TB-LMTO-ASA and FP-NMTO use average Wigner-Seitz radius 1.387 Å for Ge. For FP-NMTO, the hard sphere radius is 0.971 Å. The FP-NMTO-LDA gives a direct bandgap of 0.19 eV at Γ , which shows small improvement over LMTO+LDA of 0.10 eV. Treating the interstitial region in same way, use of improved basis set makes FP-NMTO better. However, if we switch to FP-NMTO-PBE, the bandgap is improved to 0.33 eV, but the nature of bandgap remains direct and more than 50% underestimated with respect to the experiments (0.74 eV). In contrast, the vLB-corrected LDA exchange within FP-NMTO opens up the bandgap to 0.86 eV. Importantly, the key point is the correct nature of bandgap, which is indirect along $\Gamma \rightarrow L$, now matches experiment. The valence bands remain almost same, whereas the conduction bands shift away from E_F .

For Ge in LDA and GGA, see Fig. 3, shows no key difference in band structure. The spaghetti of bands originated from the Ge-4s level were seen between -13 eV and -8.7 eV. The Ge-4p levels with a contribution of the Ge-4s level toward the less binding energies are found at the region closer to the Fermi energy (E_F). These bands extend from -8.7 eV up to 0 eV. The conduction band mainly results from Ge-4p with minor contributions of Ge-4s atomic orbitals toward the least excited states of Ge-4d from approximately 6.30 eV and up. Some degree of degeneracy is also observed depending on which direction of the BZ is traversed: in the $L \rightarrow \Gamma$, and $\Gamma \rightarrow X$

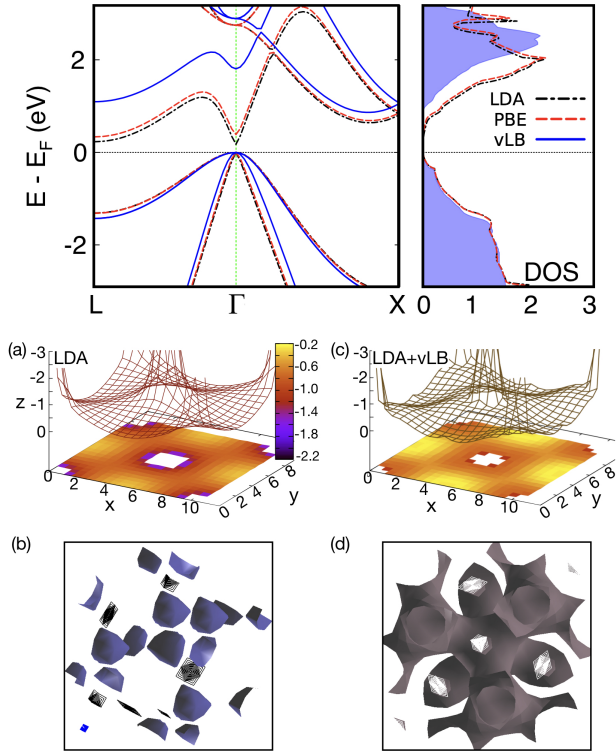


FIG. 3. (Color online) (Top) The self-consistent FP-NMTO calculated band structure (from L- Γ -X) and density of states of Ge using LDA, PBE, and LDA+vLB is shown. (Bottom) The FP-NMTO XC potential (z -axis is surface range) for (a) LDA and (c) LDA+vLB in [100]-plane. Potential-surface plots for (b) LDA & (d) LDA+vLB (isosurfaces of -0.45eV/C). Ge isosurface shows that XC potential is less local for LDA+vLB than LDA, which improves the band energies and gap.

direction. These degenerate bands belong to Ge and filled with Ge- p electrons. The Γ point has three degenerate bands; and the X point at the edge of the BZ shows two values of energies with a twofold degeneracy.

Our results show that the fundamental gap of Ge is an indirect one with the maximum of the valence band occurring at Γ and the minimum of the conduction band at the L point.² The calculated indirect gap at equilibrium lattice constant is 0.86 eV (10% overestimation with respect to experiments). The calculated direct gap at the Γ point is ~ 2.0 eV. The LDA and GGA lead to the similar and direct gap of 0.19 eV and 0.33 eV, respectively. The LDA+vLB estimated structural properties and bandgaps are in better agreement with experiments. This also shows improvement over beyond-DFT approaches.^{5,6,67,68} As the vLB potential has not been derived as a functional derivative, it is not clear what the corresponding energy is. However, the exchange energy can be evaluated by applying the virial theorem based Levy-Perdew sum rule, with this the prescription for performing DFT calculations for structural minimization with the vLB potential is complete.^{69,70}

The FP-NMTO calculated DOS, compared in Fig. 3 (right-panel), for vLB-corrected shows differences both in the energy positions and in the valence bandwidths with respect to LDA and PBE. We can see a weak shoulder at -0.60 eV followed by relatively broader peaks at -1.35 , -2.25 , and -2.9 eV and a sharper peak at -4.7 eV. In the conduction bands, a small shoulder can be found at 0.9 eV followed by a peak at 2.50 eV. Other peaks can be seen at 3.2 , 4.0 , and 4.8 eV. The position of DOS-points are in closer agreement with experiments.^{2,71-74} Even though Ge is known to be an sp material, so the correct treatment of $3d$ states is critical for accurate results. We found that major contribution of Ge- $3d$ states goes to conduction bands with smaller contribution to valence states. We consider Ge- $1s2s2p$ into the core,^{67,75} which leads to a better description of the band energies. Clearly, improving the basis set by including Ge- $3d$ states into valence achieves better energy description and (indirect) gap of Ge.

To further elaborate why vLB-corrected LDA in FP-NMTO produces better result, we plot XC-potential surface for LDA and LDA+vLB of Ge [100] plane in bottom panel of Fig 3. The z -axis is representing the strength of XC-potential in the range $\{0, -3\}$. As the nature of interstitial potential can not be understood for the full range of XC-potential, so, we show a truncated plot along z -axis. At atomic sites, the XC-potential forms deep wells, and falls exponentially to 0 in LDA (Fig.3(a)). However, the LDA+vLB shows much slower fall than LDA (Fig.3(c)). The curvature of the XC-potential surface also improves accordingly. The plots are done at isosurface values of -0.45 eV/C for both LDA and LDA+vLB in Fig.3(b),(d). This shows that the XC-potential for Ge in LDA is much more localized at the atoms, but LDA+vLB is more spread over the cell.

Bulk Gallium-arsenide: GaAs crystallizes in the zincblende ($F\bar{4}3m$) structure,⁷⁶ where Ga and As-atoms occupy $(0, 0, 0)$ and $(1/4, 1/4, 1/4)$ sites, respectively. The ES are placed to maintain the curvature of potential. We plot FP-NMTO calculated band structure and DOS in Fig. 4(a). The bandgap from LDA, PBE and LDA+vLB comes out to be 0.33 eV, 0.54 eV, and 1.43 eV, respectively. The FP-LMTO+vLB calculated bandgap of 1.43 eV shows good agreement with experimentally observed bandgap of 1.52 eV.⁷⁶ Clearly, LDA and PBE hugely underestimate the bandgap compared to LDA+vLB. Moreover, the direct (D) nature of the bandgap is also well reproduced. The band structure and DOS in Fig. 4 does not show any constant shift, which rules out any scissor operator behavior of LDA+vLB. The band structure shows larger improvement in energy levels at Γ than at X or L points. We see no change in shape of DOS except at the conduction bands near E_F and valence bands at -2.25 eV. In Fig. 4 (b),(c), the potential-energy surface for GaAs is shown along [100], where overlap between the potential spheres are determined self consistently. The z -axis shows the strength of XC potential. For clarity, we show a truncated XC-potential surface in the range

System	Si	Ge	GaP	GaSb	GaAs	InAs	InSb	InP	
a(Å) (→)	5.50	5.57	5.45	6.00	5.65	6.04	6.48	5.85	
XC(↓)	Band Gap (eV)								
LDA (NMTO)	0.79(I)	0.19(D)	1.53	0.25	0.33	0.01	0.00	0.5	
PBE (NMTO)	0.845(I)	0.33(D)	1.68	0.51	0.54	0.04	0.02	0.90	
vLB (NMTO)	1.25(I)	0.86(I)	1.87	0.94	1.43	0.39	0.79	1.18	
LB [Ref 28]	0.25	0.00	0.61	0.00	0.00	0.00	0.00	0.00	
Expt.	1.17(I)	0.74(I)	2.32	0.81	1.52	0.43	0.23	1.42	
GW ^{67,77-79}	1.31-1.29	0.65-0.71	2.80	0.62	1.58	0.31	0.08	1.44	
HGH ⁸⁰	–	–	2.44	0.55	1.01	0.19	0.21	1.23	
GDF ⁸¹	1.17	0.49	2.47	0.93	1.72	1.40	0.99	2.55	
HSE ^{82,83}	1.28	0.00	2.47	0.72	1.21	0.39	0.29	1.64	
TPSS ⁸⁴	0.82	0.56	1.98	0.08	0.52	0.00	0.00	0.90	
MBJ ²⁷⁻³¹	1.17	0.85	2.24	0.82	1.64, 1.53	0.42, 0.43	0.24, 0.25	1.59, 1.42	
HIS ⁸⁵	1.22	0.54	2.67	1.31	1.86	0.93	0.80	2.23	
EXX ⁸⁶	1.50	1.01	–	–	1.82	–	–	–	

TABLE I. FP-NMTO bandgaps for group IV and III-V materials (in eV) from LDA, PBE and LDA+vLB compared with other existing theories and experiments. For LMTO-vLB see ref.[34]. I=indirect-bandgap; D=direct-bandgap.

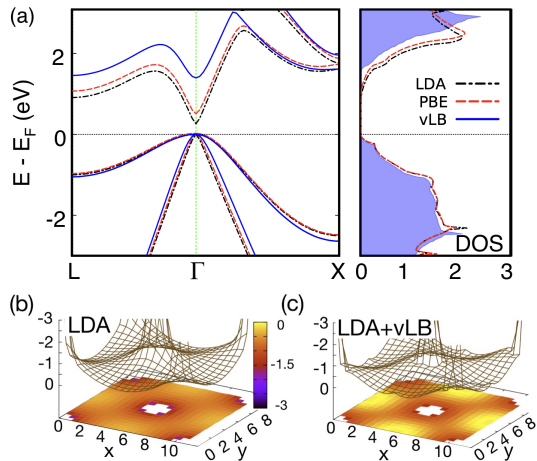


FIG. 4. (Color online) For GaAs, FP-NMTO (a) band structure along L- Γ -X (left-panel) and density of states (right-panel) with LDA, PBE and LDA+vLB. The FP-NMTO-vLB bandgap (1.43 eV) shows agreement with experiment (1.52 eV).⁷⁶ We also show the XC-potential surfaces corresponding to (b) LDA and (c) LDA+vLB in [100] plane.

$\{0, -3\}$ along z -axis. We can see that at atomic sites, the XC potential forms deep well like structure, and falls exponentially to 0, which is similar to Ge. The light yellow zone in Fig. 4(c), shows smaller interstitial contribution. This is only possible if we have smaller number of interstitial electrons than LDA (darker spots), which consequently helps correcting the energy levels in conduction band.

We summarize the bandgaps of IV and III-V semiconductors in Table I, and show that improving the basis set along with LDA+vLB yields significantly better results. As noted in the Table I, we find large discrepancy be-

tween LDA+vLB results (present calculation) and Ref. [28]. We believe that the difference comes from both due to differences in the basis sets as well the handling of the convergence of the tricky asymptotics.³⁴

A. Application to 2D materials: h -BN and h -SiC

The 2D materials, like of graphene and hexagonal boron nitride (h -BN), have drawn tremendous attention in terms of both fundamental physics and possible applications in energy-generation devices.^{87,88} Single layers of graphene and h -BN have been fabricated and found to be stable at room temperature.⁸⁹⁻⁹¹ Here, we exemplify the efficacy of our approach by discussing the electronic structure of 2D h -BN and SiC.⁹²⁻⁹⁴

2D h -BN is a group III-IV binary compound displaying interesting chemical and electronic structure properties that leads to wide range of technological applications, such as protective coating, deep ultraviolet emitter, and transparent membrane.^{98,99} 2D h -BN has similar honeycomb atomic structure as graphene with a lattice mismatch of 2%,^{100,101} where each primitive cell contains a B and N atom and share total of eight electrons. Each B (N) atom forms sp^2 hybridized state with N (B), where each state forms three in-plane σ (6-electrons) and an out-of-plane π (2-electrons) bond. The NMTO-vLB energy minimized lattice constant of 2.508 Å is in good agreement with that measured (2.504 Å).¹⁰² Unlike graphene,⁸⁸ h -BN is a wide bandgap insulator.⁹⁵ The calculated bandgap of ~ 4.5 eV, in Fig. 5(b), falls within the experimentally observed bandgap range of 3.6–6 eV.⁹⁵ The nature of bandgap can not be clearly stated as the band-energies of the lowest-occupied bands at K and M are the same, i.e., a flat band along (K-M).

Similarly, 2D h -SiC is a group IV binary compound

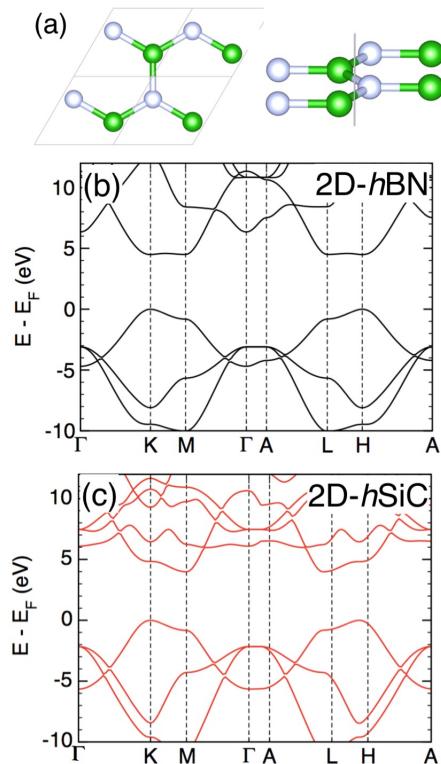


FIG. 5. (Color online) For 2D h -BN and h -SiC, the (a) (001) and (101) view of the crystal structure. The FP-NMTO-vLB band structure for (b) h -BN and (c) h -SiC plotted along high-symmetry directions in the Brillouin zone. Bandgap for h -BN of ~ 4.5 eV is in good agreement with experimentally observed range (3.6 – 6 eV).⁹⁵ The bandgap for h -SiC (3.90 eV) is overestimated compared to experiment⁹⁶ (3 eV) but most theories find similar behavior,⁹⁷ where, e.g., G_0W_0 overestimates (4.4 eV).¹⁰³

that can be viewed as graphene (2D C) or silicene (2D Si) doped with ‘Si’ or ‘C’, respectively. The honeycomb lattice of randomly but homogeneously distributed Si atoms in symmetric, semi-metallic graphene opens up a large gap. Because of its wide bandgap, h -SiC band structure has been in active study for optoelectronic applications.³⁵ Unlike the polymorphs of carbon, h -SiC is a polar material. In spite of the fact that both constituents of SiC are Group IV elements, charge is transferred from Si to C due its to higher electronegativity.

The NMTO-vLB energy minimized lattice constant of 2.62 \AA is in good agreement with the measured $a=2.6\pm 0.2 \text{ \AA}$.^{96,97} The bandgap of 3.90 eV (indirect along K to M in Fig. 5(c)) is overestimated compared to experiment (2.96 eV).⁹⁶ However, a similar trend is observed in most theoretical approaches.⁹⁷ Moreover, we found good agreement in structural behavior with experiments, while other theoretical results show significant differences, which yield a gap to be as high as 4.42 eV due to strong excitonic effects included at the G_0W_0 level of theory.¹⁰³

V. CONCLUSION

The bandgaps of IV and III-V semiconductors are underestimated by most semi-local exchange-correlation functionals. To address the problem, we combine (a) self-consistent FP-NMTO method (provide a compact and complete optimal basis throughout a supercell volume – with no approximations, e.g., for interstitial regions); with (b) vLB correction to the LDA exchange. The FP-LMTO-vLB approach provides a fast and efficient way to calculate accurate bandgaps, comparable to hybrid exchange functionals, with the speed of semilocal functionals (e.g., GGA). The combined improvement in optimal basis set (FP-NMTO) and asymptotic behavior of the exchange hole (LDA+vLB) yield much better bandgaps. The self-consistent FP-NMTO-vLB can be more effective in calculating material properties (e.g., electronic, optical), localized atomic orbitals (Wannier functions), or real-space tight-binding parameters for electronic-structure studies, as exemplified here for bandgaps in group IV and III-V semiconductors and 2D materials.

VI. ACKNOWLEDGEMENTS

S.D. and A.M. would like to thank Yoshiro Nohara and O. K. Andersen for permission to modify the FP-NMTO. S.D. is thankful to I. Dasgupta for useful discussion. Research at Ames Laboratory was funded by the U.S. Department of Energy (DOE), Office of Science, Basic Energy Sciences, Materials Science and Engineering Division, which is operated for the U.S. DOE by Iowa State University under contract DE-AC02-07CH11358.

APPENDIX:

Reproducing exact exchange behavior – Hydrogen atom problem:

The LB potential goes as $-1/r$ for densities that decay exponentially as a function of r . The effective potential $V_x + V_c + V_{LB}$ along with the LDA potential $V_x + V_c$ are shown in Fig. 6 for an electron in a hydrogen atom. We note that while the density of the electron decays as $exp(-r)$ for positions far from the origin. The exact known densities for these systems are used to obtain these potentials. The potentials are compared with the exact exchange-correlation potential given by negative of the electrostatic potential for these single-electron systems. It is clear that except close to $r = 0$, the vLB corrected potential is very close to the exact exchange-correlation potential.

The proximity of the vLB potential to the exact one also leads to much smaller error in self-interaction energy in the vLB corrected potential as shown in Table. II. In the able. II, we have displayed the exact potential

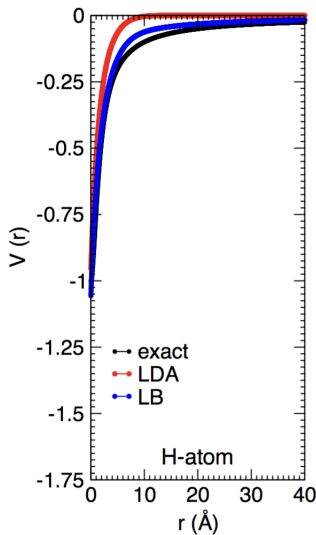


FIG. 6. (Color online). We compare the LDA+vLB potential with the exact-exchange and the LDA potentials for a single electron density. The LDA+vLB corrected potential matches closely with the exact exchange-correlation.

System	V_{exact}	V_{LB}	$\frac{(exact-LB)}{exact}$ % change	V_{LDA}	$\frac{(exact-LDA)}{exact}$ % change
H Atom	0.3144	0.2858	9.09	0.2226	29.20

TABLE II. Total energy for a single electron in a hydrogen atom obtained using the exact, LDA and LB-corrected LDA potentials. The LB-corrected LDA potential provides a significant improvement to the energy without invoking need for self-interaction corrections.

(self-interaction free) given by for a single electron system and compare exact energies calculated with V_{exact} potential with approximate exchange-correlation functional i.e., V_{LDA} or V_{LB} . We do this for an electron: the hydrogen atom. In the table below, we show that Total energy for a single electron in a hydrogen atom obtained using the exact, LDA and LB-corrected LDA potentials. Clearly, the LB-corrected LDA potential provides a significant improvement to the energy without

invoking need for self-interaction corrections.³⁶

Calculation Details –TB-LMTO-ASA

In TB-LMTO-ASA core states are treated as atomic-like in a frozen-core approximation and energetically higher-lying valence states are addressed in the self-consistent calculations of the effective crystal potential, which is constructed by overlapping Wigner-Seitz spheres for each atom in the unit cell. Two-fold criteria for generating crystal potential, on the same footings of TB-LMTO-ASA, has been used: (a) use of trial wave function, i.e., linear combinations of basis functions like plane waves in the nearly free-electron method, and (b) use of matching condition for partial waves at the muffin-tin sphere.^{104,105} We have used the LDA correlation parameterized by van Barth and Hedin⁵¹ with corrected vLB exchange, matched at the ASA radii. Following atom-sphere-approximation in TB-LMTO-ASA,¹⁰⁴, the open shell structured semiconductors are filled with empty spheres (ESs) for improved basis. Here, ESs are empty sites with no cores and small density of electronic charges. The dependence of dimensionless parameter x present in vLB correction on R_{ASA} is very crucial, so appropriate choice of R_{ASA} is important. In all calculations, we chose R_{ASA} by $\pm 5-10\%$ from default values to control the overlapping of atomic spheres and empty spheres to reduce the loss of electrons into the (unrepresented) interstitial for open-shell structures, e.g. semiconductors.

Advantage of FP-NMTO over TB-LMTO-ASA

The improved basis set of FP-NMTO method is accurate, minimal and flexible. Accurate because the FP-NMTO basis solves the KS equation exactly for overlapping muffin-tin potentials. Orthonormalized FP-NMTOs are localized atom-centered Wannier functions, generated in real space with Green-function techniques, without projection from band states.¹⁰⁶ The TB-LMTO-ASA lacks in all above. Increased computational time is the only downside of the FP-NMTO compared to TB-LMTO-ASA.

* prashant40179@gmail.com

¹ H. Droge, M. Nagelstrasser, J. Numberger, W. Faschinger, A. Fleszar, and H.-P. Steinrumck, Surf. Sci. **454**, 477 (2000).

² E. Landemark, C.J. Karlsson, L.S.O. Johansson, and R. I. G. Uhrberg, Phys. Rev. B **49**, 16523 (1994).

³ J.A. Stroschio, R.M. Feenstra, and A.P. Fein, Phys. Rev. Lett. **57**, 2579 (1986).

⁴ R.M. Feenstra, J.A. Stroschio, and A.P. Fein, Surf. Sci. **181**, 295 (1987).

⁵ W. Ku, and A.G. Eguluz, Phys. Rev. Lett. **89**, 126401 (2002).

⁶ P.V. Smith, M. Hermanowicz, G.A. Shah, and M.W. Radny, Comput. Mater. Sci **54**, 37 (2012).

⁷ H. Yutaka, I. Kojiro, Y. Akira, and K. Makoto, Jpn. J. Appl. Phys. **48**, 04C125 (2009).

⁸ J.P. Perdew, K. Burke, and M. Ernzerhof, Phys. Rev. Lett. **77**, 3865 (1996).

⁹ K. Burke, J. P. Perdew, and Y. Wang, in Electronic Density Functional Theory, edited by M. P. Das, G. Vignale, and J. F. Dobson (Plenum, New York, 1997).

- ¹⁰ J.P. Perdew, and A. Zunger, Phys. Rev. B **23**, 23, 5048 (1981).
- ¹¹ J.P. Perdew, and M. Levy, Phys. Rev. Lett. **51**, 1884 (1983).
- ¹² L.J. Sham, and M. Schlüter, Phys. Rev. Lett. **51**, 1888 (1983).
- ¹³ P. Mori-Sanchez, A.J. Cohen, and W. Yang, Phys. Rev. Lett. **100**, 146401 (2008).
- ¹⁴ W. Kohn and L. J. Sham, Phys. Rev. **140**, A1133 (1965).
- ¹⁵ J.P. Perdew et. al., Proceedings of the National Academy of Sciences, **114**(11), 2801.
- ¹⁶ A. Seidl, A. Gorling, P. Vogl, J.A. Majewski, and M. Levy, Phys. Rev. B **53** (7), 3764 (1996).
- ¹⁷ R. W. Godby, M. Schlter, and L. J. Sham Phys. Rev. B **37**, 10159 (1988).
- ¹⁸ M. K. Harbola, Phys. Rev. A **57**, 4253 (1998).
- ¹⁹ J.P. Perdew, R. G. Parr, M. Levy and J. L. Balduz Jr, Phys. Rev. Lett. **49**(23), 1691 (1982).
- ²⁰ R. Armiento, S. Kümmel, and T. Körzdörfer, Phys. Rev B **77**, 165106 (2008).
- ²¹ P. Singh, M.K. Harbola, B. Sanyal and A. Mookerjee, Phys. Rev. B **87**, 235110 (2013).
- ²² M.G. Medvedev, I.S. Bushmarinov, J. Sun, J.P. Perdew, and K.A. Lyssenko, Science **355**, 49 (2017).
- ²³ H.S. Yu, S.L. Li, and D.G. Truhlar, J. Chem. Phys. **145**, 130901 (2016).
- ²⁴ R. van Leeuwen and E.J. Baerends, Phys. Rev. A **49**, 2421 (1994).
- ²⁵ A. Savin, C.J. Umrigar and X. Gonze, Chem. Phys. Let. **288**, 391 (1998).
- ²⁶ A.D. Becke and E. R. Johnson, J. Chem. Phys. **124**, 221101 (2006).
- ²⁷ F. Tran and P. Blaha, Phys. Rev. Lett. **102**, 226401 (2009).
- ²⁸ F. Tran, S. Ehsan, and P. Blaha, Phys. Rev. Mater. **2**, 023802 (2018).
- ²⁹ D. Koller, F. Tran, and P. Blaha, Phys. Rev. B **85**, 155109 (2012).
- ³⁰ J. A. Camargo-Martinez, and R. Baquero, Phys. Rev. B **86**, 195106 (2012).
- ³¹ Y. Wang, H. Yin, R. Cao, F. Zahid, Y. Zhu, L. Liu, J. Wang, and H. Guo, Phys. Rev. B **87**, 235203 (2013).
- ³² R. Armiento and S. Kümmel, Phys. Rev. Lett. **111**, 036402 (2013).
- ³³ P. Singh, M.K. Harbola, and A. Mookerjee, *Calculation of bandgaps for bulk-and nano-materials using Harbola-Sahni and van Leeuwen-Baerends Potentials*, in *Modeling, Characterization, and Production of Nanomaterials*, Ed. V.K. Tewary, and Y. Zhang (Woodhead Publishing, Massachusetts 2015), Edition 1, Vol. 1, pp. 407-418.
- ³⁴ P. Singh, M.K. Harbola, M. Hemanadhan, A. Mookerjee, and D.D. Johnson, Phys. Rev. B **93**, 085204 (2016).
- ³⁵ B. Sadhukhan, P. Singh, A. Nayak, S. Datta, D.D. Johnson, and A. Mookerjee, Phys. Rev. B **96**, 054203 (2017).
- ³⁶ P. Singh, M.K. Harbola, and D.D. Johnson, J. Phys.: Condens. Matter **29**, 424001 (2017).
- ³⁷ T. Chachiyo and H. Chachiyo, arXiv:1706.01343 (2017).
- ³⁸ O.K. Andersen, and T. Saha-Dasgupta, Phys. Rev. B **62**, R16 219 (2000).
- ³⁹ H. Takeda, A. Chutinan, and S. John, Phys. Rev. B **74**, 195116 (2006).
- ⁴⁰ Y. Nohara, O.K. Andersen, Phys. Rev. B. **94**, 101103 (2016).
- ⁴¹ H.L. Skriver, *The LMTO Method* (Springer, New York, 1984).
- ⁴² O.K. Andersen, Phys. Rev. B **12**, 3060 (1975).
- ⁴³ O.K. Andersen, O. Jepsen, and G. Krier *Lectures in Methods of Electronic Structure Calculations, Eds.: V. Kumar, O.K. Andersen, A. Mookerjee* (World Sci. Publ. Co., Singapore, 1994).
- ⁴⁴ L. Vitos *Computational Quantum Mechanics for Materials Engineers; The EMTO Method and Applications* (Springer, London, 2007).
- ⁴⁵ O.K. Andersen, C. Arcangeli, R.W. Tank, T. Saha-Dasgupta, G. Krier, O. Jepsen, I. Dasgupta *Tight-Binding Approach to Computational Materials Science, Eds. L. Colombo, A. Gonis, P. Turchi* (MRS Symposium Proceedings Series, vol 491, 1998).
- ⁴⁶ W.R.L. Lambrecht, and O.K. Andersen, Phys. Rev. B **34**, 2439 (1986).
- ⁴⁷ S.H. Vosko, L. Wilk and M. Nusair, Can. J. Phys. **58** (8), 1200 (1980).
- ⁴⁸ F.D., Murnaghan, Proc. Natl. Acad. Sci. USA **30**, 244 (1944).
- ⁴⁹ I.N. Remediakis, and E. Kaxiras, Phys. Rev. B **59**, 5536 (1999).
- ⁵⁰ *Semiconductors. Physics of Group IV elements and III-V Compounds, Ed. K.H. Hellwege and O. Madelung, Landolt- Bornstein, New Series, Group III, Vol. 17*, (Springer, Berlin, 1982).
- ⁵¹ U. von Barth, and L. Hedin, J. Phys. Chem. **5**, 1629 (1972).
- ⁵² J.C. Slater, Phys. Rev. **81**, 385 (1951).
- ⁵³ C.O. Almbladh and U. von Barth, Phys. Rev. B **31**, 3231 (1985).
- ⁵⁴ J.P. Perdew, and Y. Wang, Phys. Rev. B **33**, 8800 (1986).
- ⁵⁵ M.K. Harbola, and V.K. Sahni, Phys. Rev. Lett. **62**, 489 (1989).
- ⁵⁶ M.K. Harbola, and V.K. Sahni, Int. J. Quantum Chem. **24**, 569 (1990).
- ⁵⁷ A. Banerjee, and M.K. Harbola, Phys. Rev. A **60**, 3599(1999).
- ⁵⁸ A.D. Becke, Phys. Rev. A **38**, 3098 (1988).
- ⁵⁹ M. van Schilfgaarde, T. Kotani, and S. V. Faleev, Phys. Rev. B **74**, 245125 (2006).
- ⁶⁰ M. Rahaman, P. Singh, A. Mookerjee, and M.K. Harbola, *The band-gap problem: An approach using the modified density functional theory and the Harbola-Sahni exchange potential*, in *Simulation and Characterization of the Advanced Materials Edition*, Ed. S. Kumar, (Transworld Research Network, 2012), Edition 1, Ch. 2, pp. 13-26.
- ⁶¹ J. B. Krieger, Yan Li, and G. J. Iafrate, Phys. Rev. A **45**, 101 (1992).
- ⁶² J. B. Krieger, Yan Li, and G. J. Iafrate, Phys. Lett. A **146**, 256 (1990).
- ⁶³ S. Kümmel and L. Kronik, Rev. Mod. Phys. **80**, 3 (2008).
- ⁶⁴ M. Lein and S. Kümmel, Phys. Rev. Lett. **94**, 143003 (2005).
- ⁶⁵ M. Mundt and S. Kümmel, Phys. Rev. Lett. **95**, 203004 (2005).
- ⁶⁶ J.S. Kasper, and S.M. Richards, Acta Crystallographica **17**, 752 (1964).
- ⁶⁷ M. Rohlfing, P. Krüger, and J. Pollmann, Phys. Rev. B **48**, 17791 (1993).
- ⁶⁸ M.S. Hybertsen, and S.G. Louie, Phys. Rev. B **34**, 5390 (1986).
- ⁶⁹ M. Levy and J.P. Perdew, Phys. Rev. A **32**, 2010 (1985).

- ⁷⁰ A. Banerjee, and M.K. Harbola, Phys. Rev. A **60**, 3599 (1999).
- ⁷¹ D.E. Eastman, W.D. Grobman, J.L. Freeouf, and M. Erbudak, Phys. Rev. B **9**, 3473 (1974).
- ⁷² D. Straub, L. Ley, and F.J. Himpsel, Phys. Rev. B **33**, 2607 (1986).
- ⁷³ D.A. Muzychenko, S.V. Savinov, V.N. Mantsevich, N.S. Maslova, V.I. Panov, K. Schouteden, and C.V. VanHaendonck, Phys. Rev. B **81**, 035313 (2010).
- ⁷⁴ W.B. Jackson, J.E. Northrup, J.W. Allen, and R.I. Johnson, Phys. Rev. Lett. **56**, 1187 (1986).
- ⁷⁵ E.L. Shirley, X. Zhu, and S.G. Louie, Phys. Rev. Lett. **69**, 2955 (1992).
- ⁷⁶ P. Villars, and K. Cenzual, *GaAs Crystal Structure: Datasheet* from “PAULING FILE Multinaries” in SpringerMaterials (Springer-Verlag Berlin Heidelberg, 2012).
- ⁷⁷ M. S. Hybertsen, and S. G. Louie, Phys. Rev. B **34**, 5390(1986), *ibid* Phys. Rev. Lett. **55**, 1418(1985).
- ⁷⁸ F. Gygi, and A. Baldereschi, Phys. Rev. Lett. **62**, 2160 (1989).
- ⁷⁹ X. Zhu, and S. G. Louie, Phys. Rev. B **43**, 14142 (1991).
- ⁸⁰ S. Q. Wang, and H. Q. Ye, J. Phys.: Condens. Matter **14**, 9579 (2002).
- ⁸¹ I. N. Remediakis, and E. Kaxiras, Phys. Rev. B **59**, 5536 (1999).
- ⁸² J. Heyd, J.E. Peralta, and G.E. Scuseria, J. Chem. Phys. **123**, 174101 (2005).
- ⁸³ J. Heyd and G.E. Scuseria, J. Chem. Phys. **121**, 1187 (2004).
- ⁸⁴ J. Tao, J. P. Perdew, V. N. Staroverov, and G. E. Scuseria, Phys. Rev. Lett. **91**, 146401 (2003).
- ⁸⁵ M. J. Lucero, T. M. Henderson, and G E Scuseria, J. Phys.: Condens. Matter **24**, 145504 (2012).
- ⁸⁶ M. Stadele, M. Moukara, J. A. Majewski, P. Vogl, and A. Görling, Phys. Rev. B **59**, 10031 (1999).
- ⁸⁷ A.H.C. Neto, F. Guinea, N.M.R. Peres, K.S. Novoselov, and A.K. Geim, Rev. Mod. Phys. **81**, 109 (2009).
- ⁸⁸ A.K. Geim, and K.S. Novoselov, Nat. Mater. **6**, 183 (2007).
- ⁸⁹ K.S. Novoselov, D. Jiang, F. Schedin, T.J. Booth, V.V. Khotkevich, S.V. Morozov, and A.K. Geim, Proc. Natl. Acad. Sci. U.S.A. **102**, 10451 (2005).
- ⁹⁰ J.C. Meyer, A.K. Geim, M.I. Katsnelson, K.S. Novoselov, T.J. Booth, and S. Roth, Nature **446**, 60 (2006).
- ⁹¹ M.H. Gass, U. Bangert, A.L. Bleloch, P. Wang, R.R. Nair, and A.K. Geim, Nat. Nanotechnol. **3**, 676 (2008).
- ⁹² P. Nath, S. Chowdhury, D. Sanyal and D. Jana, Carbon **73**, 275 (2014).
- ⁹³ S. Chowdhury, and D. Jana, Reports On Progress in Physics **79**, 126501 (2016)
- ⁹⁴ D. Jana, P. Nath and D. Sanyal, *Modification of electronic structure of graphene by Boron and Nitrogen doping*, in Graphene Science Handbook: Nanostructure and Atomic Arrangement Edited by M. Aliofkhaezrai, N. Ali, W.I. Milne, C.S. Ozkan, S. Mitura, J.L. Gervasoni, (CRC Publications, Taylor and Francis, ISBN 9781466591370, 2016), pp. 231.
- ⁹⁵ Y. Kubota, K. Watanabe, O. Tsuda, and T. Taniguchi, Science **317**, 932 (2007).
- ⁹⁶ S.S. Lin, J. Phys. Chem. C **116**, 3951 (2012).
- ⁹⁷ M.S. Sharif Azadeh, A. Kokabi, M. Hosseini, and M. Fardmanesh, Micro & Nano Letters **6**, 582 (2011).
- ⁹⁸ A. Hsu, X. Jia, S.M. Kim, Y. Shi, M. Hofmann, D. Nezich, J.F. Rodriguez-Nieva, M. Dresselhaus, T. Palacios, and J. Kong, Nano Lett. **12**, 161 (2012).
- ⁹⁹ S. Dai *et al.* Nature Nanotech. **14**, 421 (2015).
- ¹⁰⁰ Z. Liu *et al.*, Nature Nanotech. **8**, 119 (2013).
- ¹⁰¹ C.R. Dean, A.F. Young, I. Meric, C. Lee, L. Wang, S. Sorgenfrei, K. Watanabe, T. Taniguchi, P. Kim, K.L. Shepard, and J. Hone, Nature Nanotech **5**, 772 (2010).
- ¹⁰² V.L. Solozhenko, A.G. Lazarenko, J.-P. Petitet, and A.V. Kanaev, Journal of Physics and Chemistry of Solids **62**, 1331 (2001)
- ¹⁰³ H.C. Hsueh, G.Y. Guo, and S.G. Louie, Phys. Rev. B **84**, 085404 (2011).
- ¹⁰⁴ O. Jepsen and O. K. Andersen, *The Stuttgart TB-LMTO-ASA program, version 4.7*, Max-Planck-Institut für Festkörperforschung, Stuttgart, Germany (2000).
- ¹⁰⁵ O.K. Andersen, O. Jepsen, and M. Sob, in *Electronic Band Structure and Its Applications*, edited by M. Yussouff (Springer-Verlag, Berlin, 1986).
- ¹⁰⁶ M.W. Haverkort, M. Zwierzycki, and O.K. Andersen, Phys. Rev. B **85**, 165113 (2012).